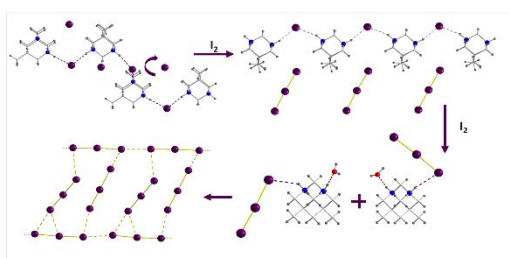# Synthesis and Supramolecular Organization of the Iodide and Triiodides of a Polycyclic Adamantane-Based Diammonium Cation: The Effect of Hydrogen Bonds and Weak I···I Interactions

Journal:	*CrystEngComm*
Manuscript ID	CE-ART-11-2020-001730.R1
Article Type:	Paper
Date Submitted by the Author:	12-Feb-2021
Complete List of Authors:	Mezentsev-Cherkes, Ivan; Lomonosov Moscow State University, Chemistry Department Shestimerova, Tatiana; Moscow State University, Chemistry Medved'ko, Alexey; Lomonosov Moscow State University, Chemistry Department; The Photochemistry Center, Kalinin, Mikhail; Moscow State University, Chemistry Kuznetsov, Alexey; Lomonosov Moscow State University Department of Chemistry, Department of Chemistry; Kurnakov Institute of General and Inorganic Chemistry RAS, Wei, Zheng; University at Albany, SUNY, Chemistry Dikarev, Evgeny V.; University at Albany, SUNY, Chemistry Vatsadze, Sergey; M.V. Lomonosov Moscow State University, Department of Chemistry Shevelkov, Andrei; Moscow State University, Chemistry

ARTICLE

Synthesis and Supramolecular Organization of the Iodide and Triiodides of a Polycyclic Adamantane-Based Diammonium Cation: The Effect of Hydrogen Bonds and Weak I···I Interactions

Ivan A. Mezentsev-Cherkess,[a] Tatiana A. Shestimerova,[a] Aleksei V. Medved'ko,[b] Mikhail A. Kalinin,[a] Alexey N. Kuznetsov, [a,c] Zheng Wei,[d] Evgeny V. Dikarev,[d] Sergey Z. Vatsadze, [a,b,†] and Andrei V. Shevelkov[a,†]

Synthesis and Supramolecular Organization of the Iodide and Triiodides of a Polycyclic Adamantane-Based Diammonium Cation: The Effect of Hydrogen Bonds and Weak I···I Interactions

Ivan A. Mezentsev-Cherkess,[a] Tatiana A. Shestimerova,[a] Aleksei V. Medved'ko,[b] Mikhail A. Kalinin,[a] Alexey N. Kuznetsov, [a,c] Zheng Wei,[d] Evgeny V. Dikarev,[d] Sergey Z. Vatsadze, [a,b,†] and Andrei V. Shevelkov[a,†]

Careful selection of organic and inorganic components allowed to produce unusual structure types with promising practical properties by facile syntheses. In this paper, we describe novel supramolecular architectures comprising organic adamantane-like divalent building blocks and iodide or polyiodide anions. Highly acidic conditions facilitated the formation of a doubly protonated organic ligand out of 5,7-dimethyl-1,3-diazaadamantane that generates three different crystal structures with inorganic counterions. In those, the cationic substructures are constructed by transforming neutral organic ligand into $[(C_{10}N_2H_{20})I]^+$ or $[(C_{10}N_2H_{20})(H_2O)]^{2+}$ cations, which crystallize with charge-compensating iodine-based anions of different complexity. All three crystal structures are characterized by various noncovalent forces ranging from strong (N)H···I, (O)H···I, and (N)H···O hydrogen bonds to secondary and week I···I interactions. Raman and diffuse reflectance spectroscopy as well as DFT calculations were employed to describe the electronic structure and optical properties of new supramolecular architectures with particular attention to the role of non-covalent interactions.

Introduction

Polyiodides have been known for many decades. They have attracted interest of many researches because of their fascinating crystal structures and a variety of applications from the century-old analytical use of iodine-starch blue to conducting polymers and Grätzel solar cells[1-3]. Recent reemergence of interest in polyiodides has evoke in the wake of the discovery of a new synthetic route to the so-called perovskite solar cells. This technique involves polyiodides as the reaction media to convert metallic lead into the light-harvesting materials.[4-6] In view of this approach, not only exploratory synthesis of polyiodides has become the topic of investigations, but other directions also emerged, including an analysis of weak bonding that governs the reactivity of polyiodides. Along these lines, investigations of supramolecular architectures involving polyiodide anions are becoming more visible, since those provide information on how a combination of multifold weak bonds may influence the overall stability of a compound and, hence, its reactivity.[7,8]

Triiodides are by far the most abundant family within the diverse class of polyiodides. Depending on the details of a particular crystal structure, they vary in geometry, being more or less symmetric, and share the common structural property, namely, the average interatomic I–I distance that span in a very narrow window of 2.91–2.94 Å [9-11]. At the same time, the involvement of triiodides into a crystal structure largely depends on their interactions with the charge-balancing cations. In the case of simple inorganic cations such as K^+, the electrostatic forces dominate. For the complex cations, other forces ensure the bonding between them and triiodide anions; those include hydrogen H···I bonds, I···I interactions of various strength, and even weak contacts between iodine and other electronegative elements, for instance, S···I [11-23].

1,3-Diazaadamantanes (DADs, Figure 1) represent the derivatives of the parent hydrocarbon, adamantane, in which two nitrogen atoms occupy the bridgehead positions of the tricyclic core in such a manner that they could affect each other due to the orbital effects. Indeed, the examination of the CSD database (See ESI, Table S1) database clearly shows that whilst the neutral DAD molecules feature more or less equal R_2N-CH_2 distances (1.470–1.475 Å), in monoprotonated and monoalkylated species these distances significantly differ, 1.399–1.430 Å for R_2N-CH_2 and 1.521–1.556 Å for R_3+N-CH_2. These data represent a clear manifestation of the anomeric effect when a nitrogen lone pair effectively donates electron density to the ▯*-orbital of the adjacent CH_2-N+R_3 bond inducing appropriate changes in N-C-N distances (Fig. 1b). The only reasonable structure of dicationic DAD contains dimethylated dications with distances R_3+N-CH_2 equal to 1.464 and 1.519 Å; however, the cation itself is asymmetric because the OH group on one of the carbon atoms is *syn* with respect to one nitrogen atom and *anti* to another one (for details, see Table S1 of ESI).

Analysis of the crystal structures of DADs reported in the literature suggests the angular nature of this dinitrogen building block; indeed, the "bite angle" between the directions of nitrogen lone pairs lies in the range of 105–106 degrees (See Table S1 of ESI). While DADs in the form of a free base could be regarded as angular di-donor supramolecular tectons (containing two acceptors of hydrogen bond), in diprotonated form they should represent angular di-acceptor tectons (containing two hydrogen bond donors).

To the best of our knowledge, no attempts have been made to explore the DAD building block in construction of the extended

a. Department of Chemistry, Lomonosov Moscow State University, 119991 Moscow, Russia.
b. N.D. Zelinsky Institute of Organic Chemistry RAS, 119991 Moscow, Russia.
c. N. S. Kurnakov Institute of General and Inorganic Chemistry RAS, 119991 Moscow, Russia.
d. Department of Chemistry, University at Albany, SUNY, Albany New York 12222, United States Address here.
† Authors for correspondence: szv@org.chem.msu.ru (SZV) and shev@inorg.chem.msu.ru (AVS).

supramolecular architectures using one or both nitrogens as electron density centers and the whole adamantane-like molecule as an angular-type linker. The di-protonated DADs have also not been documented so far.

In this work, the 5,7-dimethyl-1,3-diazaadamantane $C_{10}N_2H_{18}$ (Figure 1a) was chosen to provide a template effect in assembling new compounds with various inorganic anions made purely of iodine atoms. We present three new compounds, two of those feature a complex $[(C_{10}N_2H_{20})I]^+$ cation, which chain-like structure slightly changes to accommodate the anions of different complexity, a standalone I^- or a triiodide I_3^-, whereas the third compound features an intricate array of loosely bound I_3^- anions interacting with $[(C_{10}N_2H_{20})(H_2O)]^{2+}$ cations. A special attention is brought to hydrogen bonds that are different in strength within the complex cation and between the cations and anions as well as to interanionic $I_3^-\cdots I_3^-$ interactions.

Results and discussion

Compounds $[(C_{10}N_2H_{20})I]I$ **(1)**, $[(C_{10}N_2H_{20})I]I_3$ **(2)**, and $[(C_{10}N_2H_{20})(H_2O)](I_3)_2$ **(3)** were prepared by dissolving 5,7-dimethyl-1,3-diazaadamantane, $C_{10}N_2H_{18}$, in hydroiodic acid with a stoichiometric amount of iodine. Compound **1** forms yellowish-white polycrystalline solid, whereas **2** and **3** are obtained as needle-like brown and grey crystals, respectively. Purity of all three compounds was confirmed by comparing experimental XRD patterns with those calculated from the crystal data (See Figure S1-S3 of ESI). Compounds are stable at room **t**emperature but start to decompose upon heating at 163 (**1**), 98 (**2**), and 79 (**3**) °C (See Figures S4–S6 of ESI).

Compounds **1** and **2** crystallize in different crystal structures with dissimilar unit cell volumes of 2858 and 901 Å³, respectively (Figure 2), yet they show some common structural features. In both structures, the organic part appears as a doubly-protonated cation $C_{10}N_2H_{20}^{2+}$ linked by I^- anions into cationic chains $[(C_{10}N_2H_{20})I]^+$. The anionic parts differ in the structures of **1** and **2**. Whereas in **1** monoatomic I^- anions compensate the charge of a one-dimensional cation, in the structure of **2** the triiodide anions I_3^- serve as counterions.
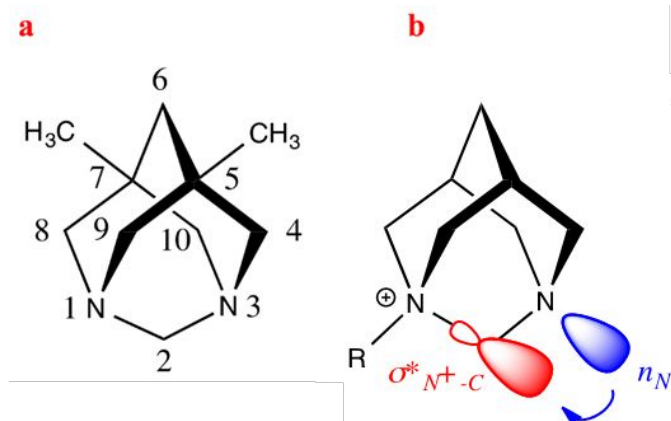

Figure 1. General view of the 1,5-dimethyl-1,3-diazaadmantane with atom numbering (a); the illustration of the anomeric effect in 1-alkylated/protonated DAD (b).
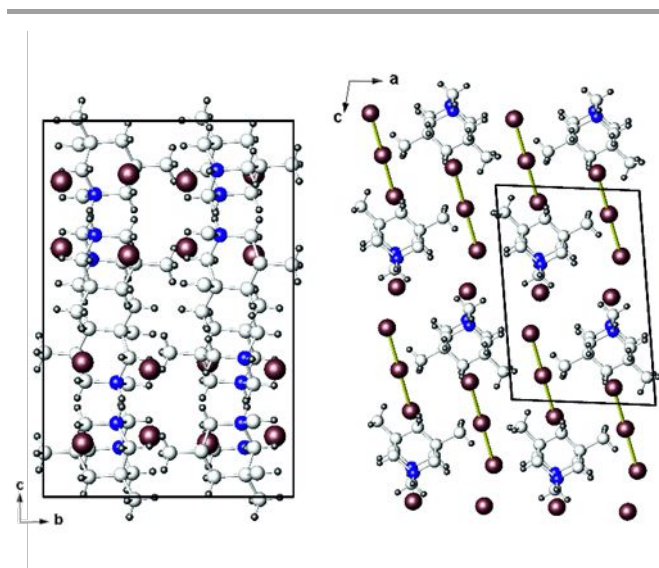

Figure 2. View of the crystal structure **1** along the *a* axis (left) and of **2** along the *b* axis (right). Iodine, brown; nitrogen, blue; carbon, light grey; hydrogen, dark grey.

The $C_{10}N_2H_{18}$ diazaadamantane is doubly protonated due to the action of strong hydroiodic acid. In both crystal structures, it transforms into the $(C_{10}N_2H_{20})^{2+}$ cation, which exploits hydrogen atoms on both nitrogens to form rather short hydrogen bonds with I^-. The (N)H···I distances range from 2.40 to 2.42 Å in **1** and from 2.50 to 2.57 Å in **2**. The former distances point to strong hydrogen bonding, which is rarely found in such systems. The latter distances also confirm the strength of the hydrogen bonds. While similar (N)H···I contacts can be found in the literature,[24] they are still considerably shorter than typical (N)H···I bonds of 2.70–2.90 Å.[25-27] As a consequence of hydrogen bonding, the cationic $[(C_{10}N_2H_{20})I]^+$ chains are formed (Figure 3). The chains are slightly dissimilar in **1** and **2** because not only the (N)H···I bonds have a different length, but also the H···I···H angles are, being 106 and 115 degrees in **1** and **2**, respectively, whereas the N–H···I angles are 159–170 degrees. Although the chains are zigzagged and run parallel to each other in both structures, they demonstrate different curvature and thus create voids of a different volume to be filled by charge-balancing anions, I^- in **1** and I_3^- in **2** (Figure 3).

The crystal structure of **3** is more complex despite of containing the same doubly-protonated 5,7-dimethyl-1,3-diazaadamantane cation, which coexists with triiodide anions and water molecules (Figure 4).

In the structure of **3**, each $(C_{10}N_2H_{20})^{2+}$ cation uses its two NH_2 groups to form two hydrogen bonds, one with water oxygen and the other with iodine of the I_3^- anion. In turn, each water molecule uses both hydrogen atoms to form hydrogen bonds with I_3^- anions. In this way, each water oxygen and each nitrogen adopt a coordination number of three and four, respectively (Figure 5). However, the strongest hydrogen bonding is formed between the diazaadamantane cation and water; the (N)H···O bonds of 1.78 Å are shorter than typical bonds of this kind, 1.8–1.9 Å. In contrast, the (N)H···I distances are quite long, ranging from 2.84 to 2.96 Å, which is significantly longer than in **1** and **2** (Table 1). The (O)H···I hydrogen bonds are also relatively long and cover the range of 2.72–2.98 Å.
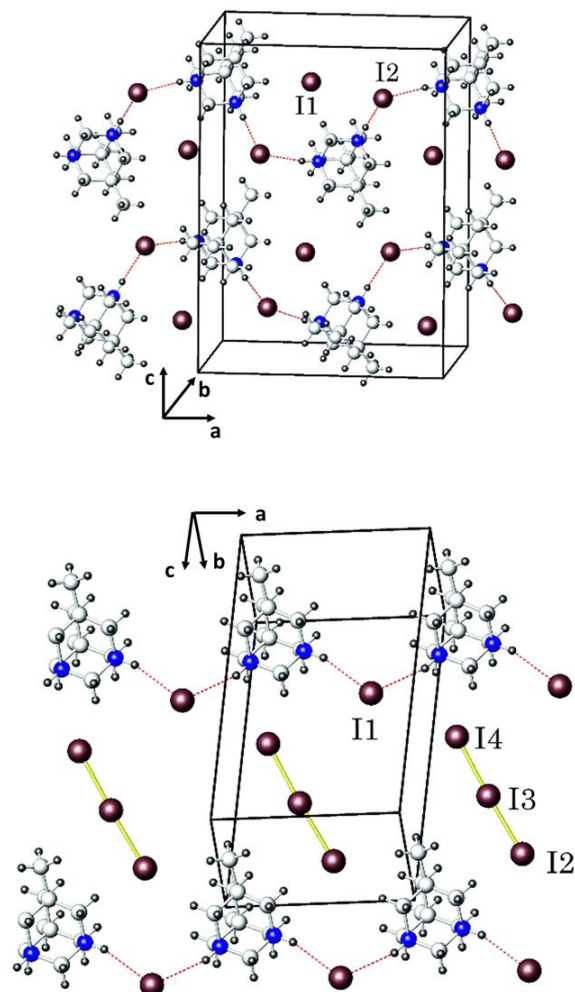
Figure 3. Zigzag cationic $[(C_{10}N_2H_{20})I]^+$ chains and guest anions in the crystal structures of **1** (top) and **2** (bottom). Iodine, brown; nitrogen, blue; carbon, light grey; hydrogen, dark grey. Hydrogen (N)H⋯I bonds are shown by dashed red lines.
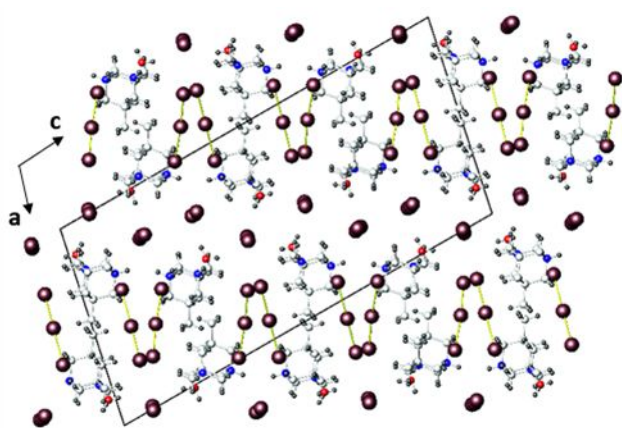

Figure 4. Projection of the crystal structure of **3** onto (*ac*) plane. Iodine, brown; nitrogen, blue; carbon, light grey; hydrogen, dark grey.

Therefore, the crystal structure of **3** can be viewed as consisting of the $[(C_{10}N_2H_{20})(H_2O)]^{2+}$ cations and twice as many I_3^- anions, yielding the charge-balanced composition $[(C_{10}N_2H_{20})(H_2O)](I_3)_2$.

The doubly-protonated diazaadamantane $(C_{10}N_2H_{20})^{2+}$ cation exhibits a symmetric N–CH$_2$–N bridge in all three crystal structures. Within the bridge, the N–C distances are 1.46–1.49 Å in the crystal structures of **1** and **3**, but are only slightly shorter, 1.45 and 1.49 Å, in **2**. For comparison, in monoprotonated diazaadamantane $(C_{10}N_2H_{19})^+$ cation, the N–CH$_2$–N bridge is highly unsymmetric; the distance from carbon to the protonated nitrogen atom is 1.54 Å, whereas the one to nitrogen baring a lone pair is only 1.42 Å.[28] We note that such asymmetry is typical for monoprotonated derivatives of the adamantane family and it is due to the anomeric effect mentioned above. For instance, in the crystal structure of urotropinium triiodide, the C–N bonds to protonated and neutral nitrogen atoms differ by nearly 0.1 Å.[29] The N–C–N angles in all three crystal structures are nearly the same; they fall in a short range of 107–109 degrees. At the same time, the N⋯N distances within the $(C_{10}N_2H_{20})^{2+}$ cation are 2.39 Å in **1**, 2.37 Å in **2**, and 2.40–2.41 Å in **3**. Those are noticeably shorter than in neutral 5,7-dimethyl-1,3-diazaadamantane, where they range from 2.44 to 2.49 Å.[30]

All three crystal structures show no sign of disorder including positioning of the anions in the voids left by the $[(C_{10}N_2H_{20})I]^+$ zigzag cationic chains in **1** and **2** or $[(C_{10}N_2H_{20})(H_2O)]^{2+}$ cations in **3**. The proper positioning of the anions is ensured by a number of weak (C)H⋯I hydrogen bonds. The (C)H⋯I distances are significantly longer than the (N)H⋯I ones and cover the range of 2.86–3.14 Å in the structure of **1**, 2.98–3.18 Å in **2**, and 3.02–3.35 Å in **3**, all these distances being typical for such kind of hydrogen bonds [25,31,32]. In total, there are eight (C)H⋯I hydrogen bonds per anion in the crystal structures of **1** and **2** (ESI, Figure S7) and from seven to eleven for four crystallographically independent I_3^- anions in **3**. The length of those hydrogen bonds points at much weaker interaction between the cations and anions in the three crystal structures compared to the (N)H⋯I bonds within the cationic chains. At the same time, even the longest distance of 3.35 Å is considerably shorter than the sum of the respective van-der-Waals radii, which can be estimated as 3.7–3.9 Å according to different sources.[33,34]

The geometry of I_3^- anion is only slightly affected by weak hydrogen bonds in **2**. The I–I distances are 2.90 and 2.91 Å, and the I–I–I angle is 177.6 deg. On a contrary, the I–I distances in **3** cover a broad range of 2.82–3.06 Å, being different in four crystallographically independent I_3^- units (Table 2). However, in all I_3^- anions in both crystal structures the average I–I distance falls within the range of 2.91–2.94 Å, typical for such anions regardless of their actual symmetry.[9–11] In accord with that, the Raman spectra of **2** and **3** (Figure 6) are almost identical and typical for asymmetric I_3^- anions;[35] they feature a strong signal at 115 cm^{-1} with an overtone near 230 cm^{-1}, which can be ascribed to the symmetric stretching of the anion. The latter is observed at 110–118 cm^{-1}, depending on the average I–I distance.[1,36,37] A weaker peak at 152 (**2**) or 161 (**3**) cm^{-1} can be attributed to the asymmetrical stretching of I_3^-, which is forbidden
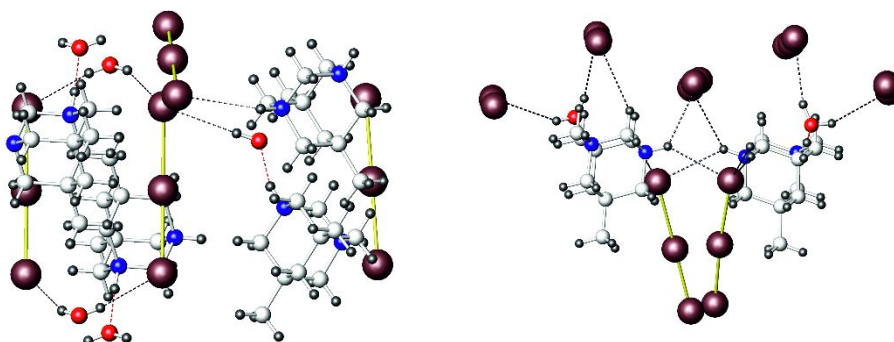
ARTICLE

Figure 5. Fragments of the crystal structure of **3** viewed along the *a* (left) and *b* (right) axes. Iodine, brown; nitrogen, blue; oxygen, red; carbon, light grey; hydrogen, dark grey. Hydrogen (O)H⋯I and (N)H⋯I bonds are shown by dashed black lines, and (N)H⋯O bonds by dashed red lines.
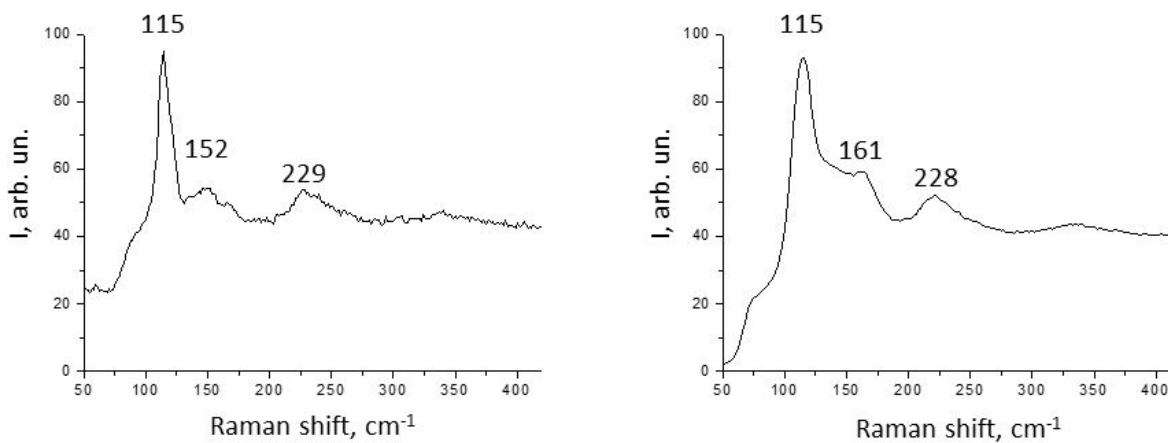

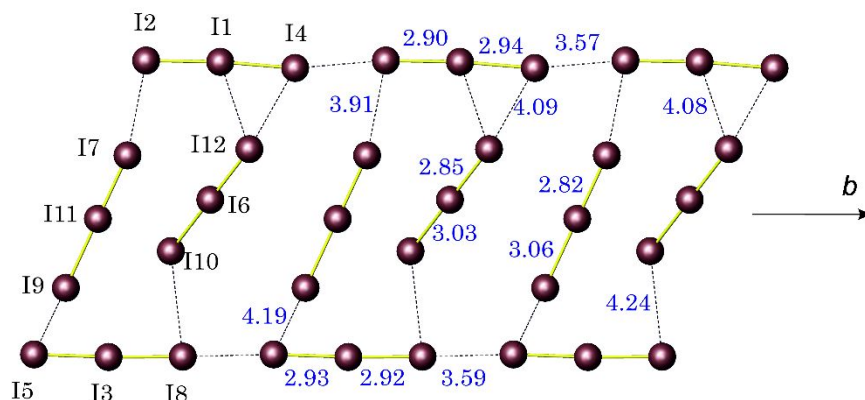Figure 6. Raman spectra of compounds **2** (left) and **3** (right).

Figure 7. Fragment of a strand composed of I_3^- anions running along the *b* axis in the crystal structure of **3**. Selected interatomic distances are shown in Å.

Table 1. Hydrogen Bonding in the Crystal Structures **1**, **2**, and **3**

D–H···A	d(H···A), Å	d(D···A), Å	angle (D–H···A),°
[(C$_{10}$N$_2$H$_{20}$)I]I (**1**)			
N1–H1···I2[a]	2.40	3.386(2)	170
N2–H2···I2[b]	2.42	3.389(2)	162
C4–H4B···I1	2.86	3.810(2)	161
[(C$_{10}$N$_2$H$_{20}$)I]I$_3$ (**2**)			
N1–H1···I1	2.50	3.445(16)	161
N2–H2···I1[c]	2.57	3.498(17)	159
C1–H1A···I3[d]	2.98	3.92(3)	162
[(C$_{10}$N$_2$H$_{20}$)(H$_2$O)](I$_3$)$_2$ (**3**)			
O1–H1C···I2[e]	2.98(9)	3.715(7)	153(11)
O1–H1D···I4	2.90(9)	3.729(7)	160(10)
O2–H2C···I5[f]	2.72(9)	3.567(8)	157(11)
O2–H2D···I4	2.74(10)	3.588(8)	153(11)
N1–H1···I8[f]	2.91	3.618(8)	128
N1–H1···I10[g]	2.84	3.633(8)	137
N3–H3···I5[f]	2.86	3.629(8)	134
N3–H···I9[g]	2.96	3.715(7)	133
N4–H4···O2[h]	1.69	2.645(12)	159
N2–H2···O1	1.78(12)	2.678(10)	175(11)

Symmetry codes: (a) -x+1/2, -y+2, z-1/2; (b) -x, -y+2, -z+1; (c) x-1, y, z; (d) x, y, z-1; (e) -x, -y, -z; (f) -x, -y+1, -z; (g) x+1, y+1, z; (h) -x+1/2, y+1/2, -z+1/2.

Table 2. Selected Interatomic Distances and Angles in the Anionic Part of the Crystal Structures **2** and **3**.

Atoms	Distance, Å	Atoms	Angle, °
[(C$_{10}$N$_2$H$_{20}$)I]I$_3$ (**2**)			
I2 – I4	2.897(3)	I4–I2–I3	177.59(10)
– I3	2.905(3)		
[(C$_{10}$N$_2$H$_{20}$)(H$_2$O)](I$_3$)$_2$ (**3**)			
I1 – I2	2.9026(9)	I2–I1–I4	176.37(3)
– I4	2.9435(9)		
I3 – I5	2.9294(9)	I8–I3–I5	177.67(3)
– I8	2.9169(10)		
I6 – I10	3.0325(10)	I12–I6–I10	175.34(3)
– I12	2.8480(10)		
I11 – I7	2.8208(10)	I7–I11–I9	179.68(3)
– I9	3.0628(10)		
O1 – H1C	0.80(8)	H1C–O1–H1D	119(10)
– H1D	0.87(8)	H2C–O2–H2D	114(10)
O2 – H2C	0.91(8)		
– H2D	0.93(8)		

for the D_{ih} symmetry but can be observed if the actual symmetry of the anion is lower.[38,39] A shoulder slightly below 90 cm^{-1}, which is poorly seen for **2** but more pronounced for **3**, is difficult to attribute, because this region of Raman shifts may reveal doubly degenerate bending vibrations of asymmetric I$_3^-$ anions (forbidden by selection rules for D_{ih} point group) and stretching vibrations of strong hydrogen bonds.

In the crystal structure of **2**, the I$_3^-$ anions are further distant from each other. On the contrary, the crystal structure of **3** features a complex arrangement of the I$_3^-$ anions, where those are building a strand running along the b axis of the unit cell (Figure 7). The strand exhibits several modes of the I$_3^-$ anions assembling with different interanionic distances. Within the anionic strand, the shortest contacts of 3.57 and 3.59 Å are observed between the anions running along the b direction in a head-to-tail fashion. Those distances are considerably longer than typical for bonds within I$_3^-$ anions but much shorter than the van der Waals contacts. Such interatomic distances are frequently observed in various polyiodides, where I$_3^-$ fragments are stacked to form one- or two-dimensional arrays. Indeed, in many triiodides, the head-to-tail I$_3^-$···I$_3^-$ contacts vary in a wide range of interatomic distances, from relatively short (near 3.2 Å) to rather long, approaching 4 Å.[40,41] Remarkably, the I···I distances of 3.57 and 3.59 Å can be compared with the intermolecular I$_2$···I$_2$ distances in crystalline diiodine, 3.50 Å, which ensure such properties of this solid as metallic luster and semiconducting behavior.[2] Generally, the interatomic I···I distances that are longer than in the I$_3^-$ anion but shorter than van der Waals contacts are called the secondary bonds.[40] Other interactions within the strand are more distant, from 3.91 to 4.24 Å; they are indicative of much weaker I$_3^-$···I$_3^-$ interactions and can be compared with the I···I van der Walls contacts, which, according to different literature sources, amount to 3.9–4.3 Å.[42]

More insight into the contribution of iodine units to the behavior of the compound, and, in particular, the role of interanionic I$_3^-$···I$_3^-$ contacts in the assembling of the crystal structure 3, can be obtained from the quantum chemical calculations data.

Calculated total and projected densities of states near the Fermi level are shown in Figure 8. As seen from the plots, the compound is a semiconductor with a band gap of *ca.* 1.25 eV. The top of the valence band, as well as the bottom of the conduction band, consist exclusively of the contributions from iodine 5p electrons. Notably, while the p-states of O, C, N, and s-states of H are mixed to a large extent, there is little to no mixing of iodine p-states with other states from the Fermi level down to *ca.* −2.5 eV. This implies that no covalent interactions occur between iodine units and other parts of the structure.

Figure 9 shows that the compound **3** is a direct-gap semiconductor; the gap is at the X point. Band dispersion is rather anisotropic in this structure, with Γ–Y and D–Z directions in the Brillouin zone showing almost flat bands (i.e. very low mobility of charge carries), and Γ–X and X–Z showing steep band slopes. This can be interpreted as the mobility of the charge carriers in this structure being mostly in the ab plane, particularly in the b-direction.

Chemical bonding in the iodine sublattice was investigated by analyzing electron localization indicator (ELI-D) topology (Figure 10).
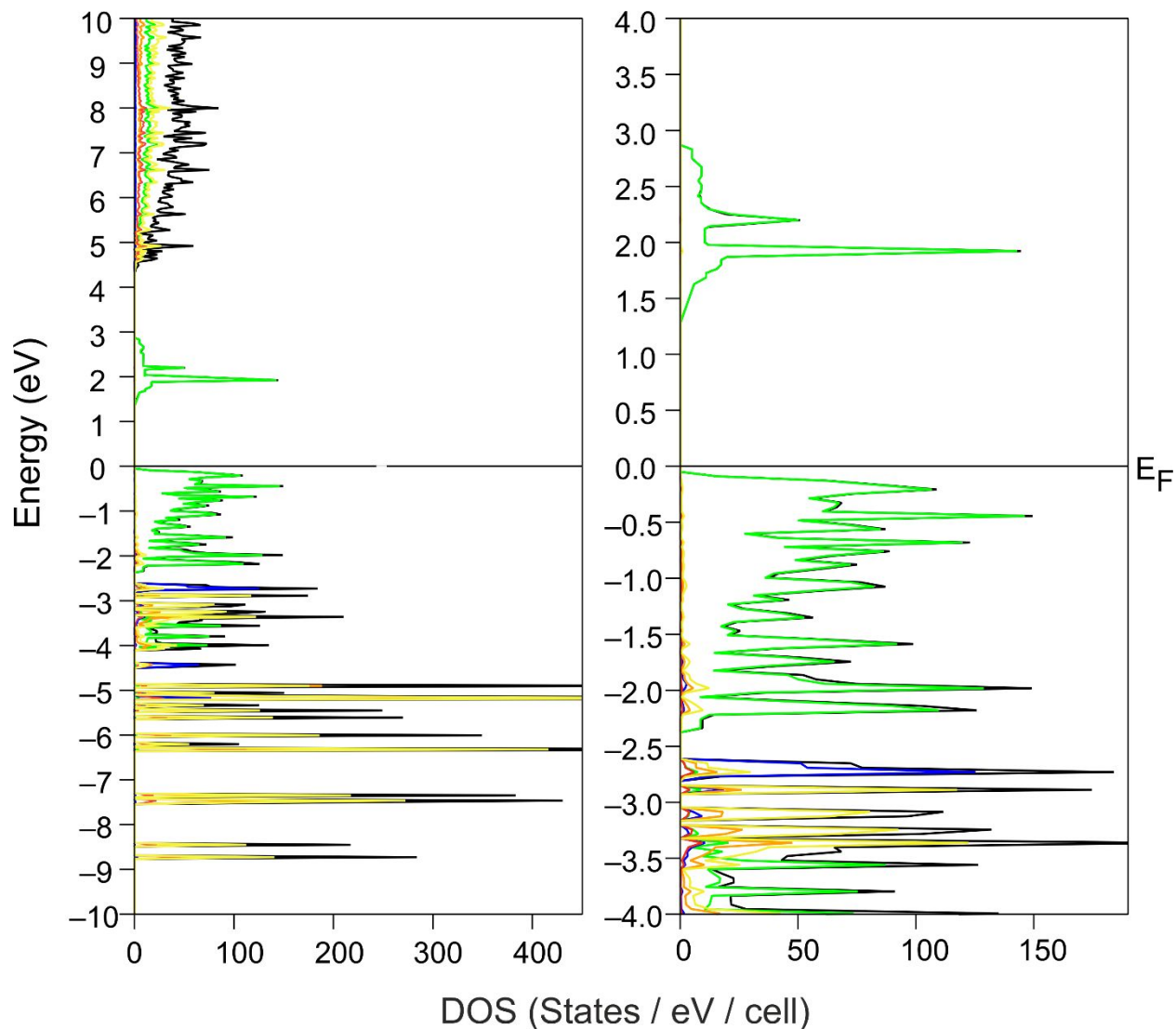
Figure 8. Total (TDOS) and projected (PDOS) densities of states near the Fermi level for **3** (full-scale and enlarged): TDOS – black, I PDOS – green, O PDOS – blue, N PDOS – orange, C PDOS – red, H PDOS – yellow.
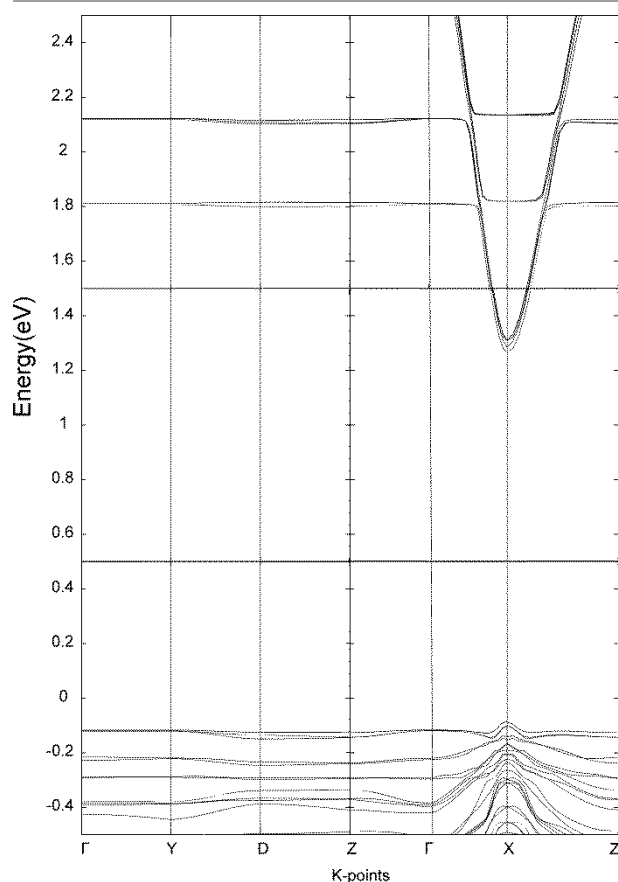
Figure 9. Calculated band structure near the Fermi level for compound **3**. The coordinates of special points are: Γ (0;0;0), Y (0;0;0.5), D (0.5;0;0.5), Z (0.5;0;0), X (0;0.5;0).

ELI-D plots confirm that the iodine network is built of the I_3^- units, which are slightly asymmetric and show one covalent I–I bond (Ω1, see Figure 10), and a third iodine atom at slightly longer distance carrying a slightly larger charge, which shows no ELI-D attractor between it and the I–I unit. The distances within the I_3^- units vary from almost equal to differ up to *ca.* 0.2 Å. This is quite typical for the I_3^- anions and is in general agreement with the description provided in the literature.[43] As ELI-D shows no indications of covalency between different I_3^- anions, weaker interactions need to be analyzed in order to reveal the nature of intermolecular forces between iodine units. A useful tool to visually analyze weak interactions is the so-called Non-Covalent Interaction (NCI) analysis based on the reduced density gradient (RDG) method.[44,45] Using this method, one can observe the regions with relatively strong attraction and weak interaction regions, which are differentiated by the electron density values (ρ(r)) – small values correspond to weak interactions (van der Waals, dispersive, etc.), and intermediate–to strong NCI – hydrogen bonds, halogen bonds, etc.

Figure 11 shows that the intramolecular and intermolecular interactions in the I_3^- units are of different nature. Within the I_3 fragments we observe a combination of covalent and halogen bonding (blue discs), which are characterized by relatively strong
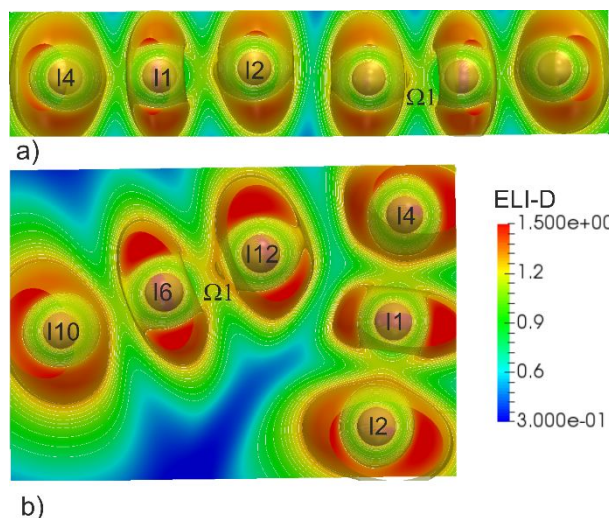

Figure 10. ELI-D sections and iso-surfaces (Y = 1.22, golden) for two modes of iodine linkage: I4–I1–I2 chains (a), and two I_3^- units at an angle (b).
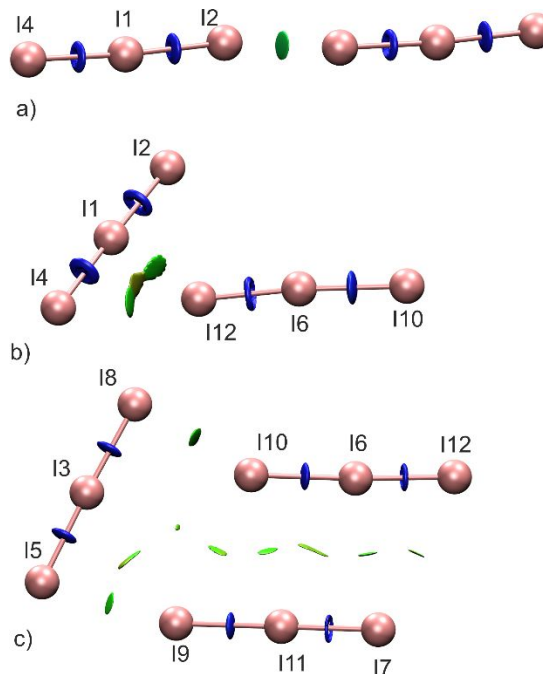

Figure 11. NCI plots for various groupings of the I_3^- units in the structure of **3** – I_3–I_3 chain (a), I_3–I_3 angle (b), I_3–I_3–I_3 group (c): blue disks represent strong interactions (halogen bonds, around bond areas), green – weak interactions (van der Waals and dispersive).

attractive forces and medium electron density. The other regions, colored in green, correspond to weak attractive forces and near-zero electron densities, i.e. weak NCI. Based on the RDG values, the strongest of these NCIs are the I2–I4 interactions, which provide the linking of the I_3^- anions into chains along the *b*-direction. Weaker NCI link I12–I6–I10 and I4–I1–I2 units through van der Waals interactions

between I12–I4 and I12–I1 (see Figure 11b). And the weakest van der Waals interactions combine three [I_3] units shown in Figure 11c into a 2D network. These fragments are not fully planar, but they do mostly reside in the *ab* plane. Therefore, this picture correlates well with the band structure, which has shown that charge carriers are mostly mobile along the *b* direction and in the *ab* plane. And thus, we can describe the iodine sublattice as a 2D network based on the NCI interactions of varying strength.

Black color of compounds **2** and **3** corresponds well to the results of the optical diffuse reflectance spectroscopy. Extrapolation of the linear part of the Kubelka-Munk plot[46] onto the energy axis gives the value of 1.37 eV for both compounds in the direct band gap approximation (ESI, Figure S8). Notably, the latter resembles the band gap in crystalline iodine (1.3 eV), which shows that non-covalent interactions facilitate and support the arrangements of structural units into a motif that has electron transport properties similar to those of crystalline iodine. Therefore, their contribution to the properties of the compound is essential and at least as important as that of the covalent contacts.

Experimental

5,7-dimethyl-1,3-diazaadamantane-6-one. Urotropine (56.00 g, 400 mmol) was dissolved in a mixture of 200 mL of *n*-butanol and 45 mL of acetic acid, and pentanone-3 (42.80 mL, 400 mmol) was added. The reaction mixture was refluxed for 3 h. All volatiles were removed on rotary evaporator, and the resulting red oil was extracted 6 times by 220 mL of hot heptane. The extract was purified by hot filtration through basic alumina and evaporated. The orange powder was dissolved in 223 mL of DCM and washed twice with 22 mL of water. The organic layer was separated, dried over sodium sulfate, and evaporated to dryness. The yield of pink powder was 48.27 g (67%).

^{1}H-NMR (400 MHz, δ, ppm, $CDCl_3$) 0.89 (6H, s, CH_3), 3.04 (4H, d, ^3J = 12.59 Hz, CH_2), 3.27 (4H, d, ^3J = 12.59 Hz, CH_2), 4.13 (2H, s, CH_2). ^{1}H-NMR spectrum is consistent with the literature data[47].

5,7-dimethyl-1,3-diazaadamantane. 5,7-Dimethyl-1,3-diazaadamantane-6-one (1.80 g, 10 mmol) was dissolved in a mixture of hydrazine hydrate (15.12 mL), sodium hydroxide (1.51 g, 38 mmol) and ethylene glycol (7.6 mL) upon heating. The reaction mixture was refluxed for 16 h. All volatiles were distilled from the reaction mixture upon heating up to 135°C. The distillate was extracted with petroleum ether (75 mL), dried over sodium sulfate, and evaporated to dryness. The yield of white powder was 0.89 g (53%).

^{1}H-NMR (400 MHz, δ, ppm, $CDCl_3$) 0.63 (6H, s, CH_3), 1.48 (2H, s, CH_2), 2.78 (4H, d, ^3J = 12.47 Hz, CH_2), 2.93 (4H, d, ^3J = 12.35 Hz, CH_2), 3.96 (2H, s, CH_2). ^{1}H-NMR spectrum is consistent with the literature data[48].

Compounds 1-3. The synthesis of the compounds **1-3** was performed using solution of hydroiodic acid (stabilized), which was prepared by hydrolysis of freshly synthesized PI_3; details of this procedure can be found elsewhere[49]. The HI acid (stabilized) was distilled at 126 °C, and the resulting solution was diluted with distilled water to required concentrations.

[($C_{10}N_2H_{20}$)I]I (**1**) was prepared by dissolving 0.1 g of 5,7-dimethyl-1,3-diazaadamantane in 2 mL of 50% HI. After 48 hours, yellowish-white plate crystals were isolated from the solution. Compound **1** is stable in humid air over weeks.

[($C_{10}N_2H_{20}$)I]I_3 (**2**) was synthesized in the solution prepared from 2 mL of H_2O, 0.2 mL of HI (50 wt%), and I_2 (0.1530 g). 5,7-Dimethyl-1,3-diazaadamantane (0.1 g) was added to the solution, which was then kept under parafilm for 96 hours. Brown needle crystals were separated by filtration under vacuum and dried at room temperature. Compound **2** is stable in open air over several weeks.

[($C_{10}N_2H_{20}$)(H_2O)](I_3)$_2$ (**3**) was obtained in the same way as **2**, but by increasing the amount of iodine twice. The resulting solid formed as grey needle-like crystals with a yellowish luster. Compound **3** is stable in air at 4-6 °C for several months; at room temperature the discoloration of solid is observed within several days.

Thermal analysis. Thermogravimetric analysis was performed using a NETZSCH 209 F1 Libra thermobalance. Samples were heated in alumina crucibles under dry nitrogen flow up to 673 K with the heating rate of 5 or 10 K·min^{-1}. The NETZSCH Proteus Thermal Analysis program was used for the data processing.

Powder X-ray diffraction analysis (PXRD) was performed on an Imaging Plate Guinier Camera (Huber G670, Cu-K$_{\alpha1}$ radiation, λ = 1.540598 Å). The data were collected by scanning the image plate 4 times upon an exposure time of 1200 s at room temperature in the 2θ range of 3–100 deg. For the data collection, crystals were finely crushed in an agate mortar, and the resulting powder was fixed on a holder using a scotch tape.

Crystal structure determination. Well-shaped single crystals of **1** and **3** were selected from the respective synthetic samples. The single crystal diffraction data were measured at 100(2) K on a Bruker D8 VENTURE with PHOTON 100 CMOS detector system equipped with a Mo-target X-ray tube (0.71073 Å). A frame width of 0.50 ° and an exposure time of 15 s/frame were employed for data collection. Data reduction and integration were performed with the Bruker software package SAINT (Version 8.38A).[50] Data were corrected for absorption effects using the semi-empirical methods (multi-scan) as implemented in SADABS (version 2018/2)[51] for **1**, and numerical methods for **3**. The crystal structures were solved by the intrinsic phase methods using the SHELXT (version 2018/2) program package,[52] which gave positions of iodine atoms. Positions of nitrogen and carbon atoms were found from successive difference Fourier syntheses. The crystal structures were refined in anisotropic approximations of atomic displacement parameters for all atoms except hydrogens. The hydrogen atoms of the cations were calculated and further refined using riding models for both structures. Three of four hydrogen atoms positions in two H_2O molecules for **3** were found from difference Fourier syntheses, the position of the last hydrogen atom was calculated from geometric considerations. All four hydrogen

ARTICLE

Table 3. Data Collection and Structure Refinement Parameters for Compounds **1**, **2**, and **3**.

Parameters	$[(C_{10}N_2H_{20})I]I$ (1)	$[(C_{10}N_2H_{20})I]I_3$ (2)	$[(C_{10}N_2H_{20})(H_2O)](I_3)_2$ (3)
Crystal system	Orthorhombic	triclinic	monoclinic
Space Group	*Pbca* (No. 61)	*P*ī (No. 2)	*P*2$_1$/*n* (No. 14)
a, Å	13.3082(8)	8.1345(12)	15.2610(19)
b, Å	11.9672(8)	8.6866(16)	9.3873(12)
c, Å	17.9425(11)	13.0650(10)	31.291(4)
α,°	90	95.775(9)	90
β,°	90	98.828(10)	101.966(2)
γ,°	90	96.093(10)	90
V, Å^3	2857.6(3)	900.7(2)	4385.3(10)
Z	8	2	8
d_{calc}	1.962	2.492	2.871
Diffractometer	Bruker D8 Venture PHOTON 100 CMOS	IPDS Stoe Pilatus100 K	Bruker D8 Venture PHOTON 100 CMOS
Radiation/wavelength	MoKα/0.71073	MoKα/0.71073	MoKα/0.71073
Temperature, K	100(2)	293(2)	100(2)
Crystal form	plate	needle	needle
Crystal size, mm	0.03×0.09×0.18	0.01×0.01×0.10	0.018×0.09×0.189
Absorption correction	multi-scan	multi-scan	numerical
θ range (data collection)	3.061-32.090	1.589-28.745	2.755-28.731
Range of *h, k, l*	−19→*h*→19; −17→*k*→17; −26→*l*→26	−10→*h*→10; −11→*k*→11; −17→*l*→17	−20→*h*→20; -12→*k*→12; -42→*l*→42
R_{int}	0.0581	0.142	0.0773
R/R_w	0.0314/0.0415	0.0527/0.1616	0.0579/0.0887
GoF	1.118	0.664	1.178
No. of params. / reflections	130/4984	147/4133	358/11337
$\Delta\rho_{max}$ (e/Å^{-3}) positive/negative	0.65/−0.68	0.83/−0.87	1.765/-1.969

atomic positions were refined freely with their isotropic atomic displacement parameters restricted to 1.5 times of their parent oxygen atom equivalent isotropic displacement parameters restricted to 1.5 times of their parent oxygen atom equivalent isotropic displacement parameter. The H–O bond distances were restrained to 0.82 Å with an estimated standard deviation of 0.02 Å.

The X-ray diffraction data for single crystals of **2** were collected at 293 K using a STOE STADI VARY diffractometer equipped with a Pilatus100K detector using a rotation method, a collimating mirror, and Mo Kα (0.71073 Å) radiation. STOE X-AREA software was used for the cell refinement and data reduction. Data collection and image processing were performed with X-Area 1.67 (STOE&Cie GmbH, Darmstadt, Germany, 2013). The intensity data were scaled up with LANA (part of X-Area) to minimize differences of intensities of symmetry-equivalent reflections (multi-scan method). The structures were solved and refined with SHELX program.[52] The non-hydrogen atoms were refined by using the anisotropic full matrix least-square procedure. The hydrogen atoms of the cations were calculated and further refined using the riding models. Low intensity of the collected reflections led to low fraction of reflections used in the refinement. Since all crystals checked showed the same problem, the crystal structure was additionally confirmed by Rietveld refinement of X-ray powder diffraction data using Jana2006 programs.[53] For more details, see ESI, Figure S3 and Table S3.

The summary of experimental and crystallographic information for compounds **1**-**3** is given in the Table 3. Selected interatomic distances and hydrogen bonding are shown in Tables 1 and 2,

respectively. Full lists of interatomic distances within cations are placed in ESI (Table S2).

CCDC 2022254, 2022255, and 2022256 (single crystals of compounds **1**, **3**, and **2**, respectively) and 2034417 (powder, compound **2**) contain the supplementary crystallographic data for this paper. These data can be obtained free of charge via www.ccdc.cam.ac.uk/data_request/cif, or by emailing data_request@ccdc.cam.ac.uk, or by contacting The Cambridge Crystallographic Data Centre, 12 Union Road, Cambridge CB2 1EZ, UK; fax: +44 1223 336033.

Raman spectroscopy. Raman spectra of compounds **2** and **3** were recorded on a Renishaw In Via spectrometer with laser wavelength of λ = 514 nm (Ar, 50 mW). Sample investigations were performed in the backscattering geometry using a confocal microscope Leica DMLM (100´ lens) at room temperature in air. Focus distance was 250 mm, and the size of laser beam was 20 μm. The CCD-camera (1024×368 pixels) was used as a detector. The scale calibration was done using monocrystalline silica (521.5 cm^{-1}) as a standard sample. WiRE 3.4 software was used for data processing.

Optical Spectroscopy. Optical diffuse reflectance spectra were recorded using a UV-vis spectrometer Perkin-Elmer Lambda 950 (Perkin-Elmer, Waltham, MA, US) with an attached diffuse reflectance accessory. Measurements were performed at 298 K in the spectral range of 250–1200 nm, with a scanning rate of 2 nm/s using finely ground polycrystalline samples. The data were transformed into absorbance using the Kubelka–Munk method and plotted as $[(k/s)\cdot h\upsilon]^2$ against $h\upsilon$, where k is the absorption coefficient, s is the scattering coefficient, and h is the Planck constant. Optical band gap, E_g, was approximated by extrapolation to k = 0.

Electronic structure calculations and bonding analysis. DFT calculations on the 3D structure of **3** were performed using the projector augmented wave method (PAW) as implemented in the Vienna Ab initio Simulation Package (VASP).[54,55] The Perdew-Burke-Ernzerhof exchange-correlation functional (PBE)[56] of the GGA type was used for the calculations, with a Brillouin zone sampling employing a Monkhorst-Pack[57] grid of 10×8×4 k-points. The PBE exchange-correlation functional has proven to be a robust choice for periodic calculations on similar systems; for instance, see a recent paper by Hu et al. on copper polyiodides.[58] Energy cutoff was set to 450 eV, and the energy convergence criterion was at 10^{-5} eV. Convergence towards the k-point set and energy was checked. DFT calculations on the iodine fragments were performed using hybrid B3LYP[59] functional, which is standard for molecular system studies, and def2-QZVPPD basis set[60] (28 e$^-$ core ECP28MDF)[61] utilizing Orca 4.2.0 package.[62,63] In both types of calculations, dispersion correction DFT-D3 by Grimme was used.[64] Chemical bonding analysis was performed *via* studying the QTAIM charge density (3D structure), Electron Localizability Indicator (ELI-D, molecular calculations)[65] and RDG (non-covalent interactions, NCI, molecular calculations)[66] topology. Topological analysis of charge density and ELI-D were performed using DGrid 4.6 package,[67] NCI analysis was performed using Multiwfn 3.7 package.[68] ELI-D was visualized using VESTA 3 package,[69] NCI plots were done using VMD 1.9.3.[70]

Conclusions

We have shown that, at the highly acidic conditions, 5,7-dimethyl-1,3-diazaadamantane could be doubly protonated giving rise to supramolecular building blocks $[(C_{10}N_2H_{20})I]^+$ and $[(C_{10}N_2H_{20})(H_2O)]^{2+}$. Depending on the slightly varying synthetic conditions, these blocks are involved in the formation of supramolecular architectures $[(C_{10}N_2H_{20})I]I$ (**1**), $[(C_{10}N_2H_{20})I]I_3$ (**2**), and $[(C_{10}N_2H_{20})(H_2O)](I_3)_2$ (**3**), in which the anionic inorganic part is made purely of iodines. Those architectures feature a number of non-covalent interactions both within the cationic and anionic parts as well as between cations and anions, which include remarkably short (N)H⋯I, (O)H⋯I, and (N)H⋯O hydrogen bonds as well as I⋯I interactions in the anionic substructure of $[(C_{10}N_2H_{20})(H_2O)](I_3)_2$ (**3**). The latter structure features the strand-shaped anionic substructure, in which I_3^- anions are linked together by intermolecular forces of different strength, ranging from secondary I⋯I interactions of 3.57–3.59 Å to week I⋯I interactions at the distances above 3.9 Å.

The analysis of the electronic structure of compound **3** allows one to evaluate regions with covalent and strong non-covalent interactions (halogen bonds) as well as regions with weak interactions related to dispersive forces; however, the band structure confirms that even week interactions contribute to the enhanced mobility of charge carriers. Also, these new materials are highly prominent for their stability in a strong acidic media; as such they can serve as precursors for the conversion of metallic lead into perovskite-like iodoplumbates that are used as light-harvesting materials in solar cells.

Author Contributions

All authors have given approval to the final version of the manuscript.

Conflicts of interest

There are no conflicts to declare.

Acknowledgements

Funding Sources

Notes and references

1. P. H. Svensson, L. Kloo, *Chem. Rev.*, 2003, **103**, 1649-1684.
2. A. Hagfeldt, G. Boschloo, L. Sun, L. Kloo, H. Pettersson, *Chem. Rev.*, 2010, **110**, 6595-6663.
3. M. Grätzel, *Inorg. Chem.*, 2005, **44**, 6841-6851.
4. I. Turkevych, S. Kazaoui, N. A. Belich, A. Y. Grishko, S. A. Fateev, A. A. Petrov, T. Urano, S. Aramaki, S. Kosar, M. Kondo, E. A. Goodilin, M. Grätzel, A. B. Tarasov, *Nat. Nanotech.*, 2019, **14**, 57-63.
5. A. A. Petrov, N. A. Belich, A. Y. Grishko, N. M. Stepanov, S. G. Dorofeev, E. G. Maksimov, A. V. Shevelkov, S. M. Zakeeruddin, M. Grätzel, A. B. Tarasov, E. A. Goodilin, *Materials Horizons*, 2017, **4**, 625-632.
6. N. A. Belich, A. A. Petrov, P. O. Rudnev, N. M. Stepanov, I. Turkevych, E. A. Goodilin, A. B. Tarasov, *ACS Appl. Mater. Interfaces,* 2020, **12**, 20456-20461.
7. T.A. Shestimerova, A.V. Shevelkov, *Russ. Chem. Rev.*, 2018, **87**, 28-48.
8. E. V. Bartashevich, V. G. Tsirelson, *Russ. Chem. Rev.*, 2014, **83**, 1181-1203.
9. J. Rusnik, S. Swen-Walstra, T. Migchelsen, *Acta Crystallogr.* 1972, **B28**, 1331-1335.
10. E. V. Savinkina, B. N. Mavrin, D. V. Albov, V. V. Kravchenko, M. G. Zaitseva, *Russ. J. Coord. Chem.*, 2009, **35**, 96-100.
11. T. A. Shestimerova, M. A. Bykov, Z. Wei, E. V. Dikarev, A. V. Shevelkov, *Russ. Chem. Bull., Int. Ed.*, 2019, **68**, 1520-1524.
12. T. A. Shestimerova, N. A. Yelavik, A. V. Mironov, A. N. Kuznetsov, M. A. Bykov, A. V. Grigorieva, V. V. Utochnikova, L. S. Lepnev, A. V. Shevelkov, *Inorg. Chem.*, 2018*,* **57***,* 4077-4087.
13. T. A. Shestimerova, N. A. Golubev, N. A. Yelavik, M. A. Bykov, A. V. Grigorieva, Z. Wei, E. V. Dikarev, A. V. Shevelkov, *Cryst. Growth Desig,* 2018, **18**, 2572-2578.
14. S. A. Adonin, A. N. Usoltsev, A. S. Novikov, B. A. Kolesov, V. P. Fedin, M. N. Sokolov, *Inorg. Chem.*, 2020, **59**, 3290-3296.
15. S. A. Adonin, A. S. Novikov, M. N. Sokolov, *Eur. J. Inorg. Chem.*, 2019, 4221-4223.
16. A. Starkholm, L. Kloo, P. H. Svensson, *ACS Appl. Energy Mater.*, 2019, **2**, 477-485.
17. G. J. Reiß, J. S. Engel, *CrystEngComm*, 2002, **4**, 155-161.
18. O. I. Bol'shakov, I. D. Yushina, E.V. Bartashevich, Y.V. Nelyubina, R. R. Aysin, O. A. Rakitin, *Struct. Chem.*, 2017, **28** (6), 1927-1934.
19. A. Abate, M. Brischetto, G. Cavallo, M. Lahtinen, P. Metrangolo, T. Pilati, S. Radice, G. Resnati, K. Rissanen, G. Terraneo, *Chem. Commun.*, 2010, **46**, 2724-2726.
20. A. N. Usoltsev, A. S. Novikov, B. A. Kolesov, K. V. Chernova, P. E. Plyusnin, V. P. Fedin, M. N. Sokolov, S. A. Adonin, *J. Mol. Struct.*, 2020, **1209**, 127949.
21. I. D. Yushina, N. M. Tarasova, D. G. Kim, V. V. Sharutin, E. V. Bartashevich, *Crystals*, 2019, **9**, 506-519.
22. E. V. Bartashevich, S. E. Mukhitdinova, I. D. Yushina, V. G. Tsirelson, *Acta Cryst. Sect. B*, 2019, **B75**, 117-126.
23. A. Peuronen, H. Rinta, M. Lahtinen, *CrystEngComm*, 2015, **17**, 1736-1740.
24. J. Zhang, S. Han, C. Ji, W. Zhang, Y. Wang, K. Tao, Z. Sun, J. Luo, *Chem. Eur. J.*, 2017, **23**, 17304-17310.
25. T. Li, Y. Hu, C. A. Morrison, W. Wu, H. Hana, N. Robertson, *Sustainable Energy Fuels*, 2017, **1**, 308-316.
26. M. Węcławik, P. Szklarz, W. Medycki, R. Janicki, A. Piecha-Bisiorek, P. Zieliński, R. Jakubas, *Dalton Trans.*, 2015, **44**, 18447-18458.
27. T. Sun, F. Liang, X. Zhang, H. Tu, Z. Lin, G. Zhang, Y. Wu, *Polyhedron*, 2017, **127**, 478-488.
28. H. Cui, R. Goddard, K.-R. Porschke, *J. Phys. Org. Chem.,* 2012, **25**, 814-827.
29. K.-F. Tebbe, K. Nagel, *Z. Anorg. Allg. Chem.,* 1995, **621**, 225-228.
30. N. S. Zefirov, V. A. Palyulin, O. I. Levina, K. A. Potekhin, E. N. Kurkutova, Y. T. Struchkov, *Vestn. Mosk. Univ., Ser. 2: Khim.*, 1987, **28**, 276.
31. B.-G. Chen, *J. Clust. Sci.*, 2017, **28**, 983-994.
32. J.-H. Lee, N. C. Bristowe, P. D. Bristowe, A. K. Cheetham, *Chem. Commun.,* 2015, **51**, 6434-6437.
33. S. Alvarez, *Dalton Trans.*, 2013, **42**, 8617-8636.
34. I. Yu. Chernyshov, I. V. Ananyev, E. A. Pidko, *ChemPhysChem.*, 2020, **21**, 370-376.
35. N. Yamanaka, R. Kawano, W. Kubo, N. Masaki, T. Kitamura, Y. Wada, M. Watanabe, S. Yanagida, *J. Phys. Chem. B*, 2007, **111***,* 4763-4769.
36. I. D. Yushina, V. I. Batalov, E. V. Bartashevich, A. O. Davydov, P. S. Zelenovskiy, A. Masunov, *J. Raman Spectrosc.*, 2017, **48**, 1411-1413.
37. P. Deplano, J. R. Ferraro, M. L. Mercuri, E. F. Trogu, *Coord. Chem. Rev.*, 1999, **188**, 71-95.
38. S. Saha, H. Okajima, O. Homma, H. Hamaguchi, *Spectrochim. Acta Part A Mol. Biomol. Spectrosc.*, 2017, **176**, 79-82.
39. P. H. Svensson, L. Kloo, *J. Chem. Soc. Dalton Trans.*, 2000, 2449-2455.
40. L. Kloo, J. Rosdahl, P. H. Svensson, *Eur. J. Inorg. Chem.*, 2002, 1203-1209.
41. J. M. Williams, H. H. Wang, T. J. Emge, U. Geiser, M. A. Beno, P. C. W. Leung, K. D. Carlson, R. J. Thorn, A. J. Schultz, *Progr. Inorg. Chem.*, 1987, **35**, 51-218.
42. P. Pyykko, *Chem. Rev.*, 1997, **97**, 597-636.
43. G. A. Landrun, N. Goldberg, R. Hoffmann, *J. Chem. Soc., Dalton Trans.*, 1997, 3605-3613.
44. E. R. Johnson, S. Keinan, P. Mori-Sánchez, J. Contreras-García, A. J. Cohen, W. Yang, *J. Am. Chem. Soc.*, 2010, **132**, 18, 6498-6506.
45. R. A. Boto, J. Contreras-Garcia, J. Tierny, J.-P. Piquemal, *Mol. Phys.*, 2015, **114***,* 1406-1414*.*
46. P. Kubelka, F. Munk, *Z. Tech. Phys. (Leipzig)*, 1931, **12**, 593-601.
47. A. V. Medved'ko, B. V. Egorova, A. A. Komarova, R. D. Rakhimov, D. P. Krut'ko, S. N. Kalmykov, S. Z. Vatsadze, *ACS Omega*, 2016, **1** (5), 854-867.
48. P. Comba, L. Daumann, J. Lefebvre, G. Linti, B. Martin, J. Straub, T. Zessin, *Aust. J. Chem.*, 2009, **62** (10), 1238-1245.
49. N.A. Yelovik, A.V. Mironov, M.A. Bykov, A.N. Kuznetsov, A.V. Grigorieva, Z. Wei, E.V. Dikarev, A.V. Shevelkov, *Inorg. Chem.*, 2016, **55**, 4132-4140.
50. *SAINT,* Version 8.38A; Bruker AXS Inc.: Madison, WI, USA, 2019.
51. L. Krause, R. Herbst-Irmer, G.M. Sheldrick, D. Stalke, *J. Appl. Cryst.*, 2015, **48**, 3-10.

52. G.M. Sheldrick, SHELXT–Integrated space-group and crystal-structure determination. *Acta Cryst.* 2015, **C71**, 3-8.

53. V. Petricek, M. Dusek, L. Palatinus, *Z. Kristallogr. – Cryst. Mater.*, 2014, **229**, 345-352.

54. G. Kresse, D. Joubert, *Phys. Rev. B*, 1999, **59**, 1758-1775.

55. G. Kresse, J. Furthmüller, Vienna Ab initio simulation package (VASP), v.5.3, http://www.vasp.at/.

56. J.P. Perdew, K. Burke, M. Ernzerhof, *Phys. Rev. Lett.*, 1996, **77**, 3865.

57. H. J. Monkhorst, J. D. Pack, *Phys. Rev. B*, 1976, **13**, 5188-5192.

58. J. Hu, J. Zhou, S. Cao, *Dalton Trans.*, 2018, **47**, 17216-17220.

59. A.D. Becke, *J. Chem. Phys.*, 1993, **98**, 5648.

60. D. Rappoport, F. Furche, *J. Chem. Phys.*, 2010, **133**, 134105.

61. B. Metz, H. Stoll, M. Dolg, *J. Chem. Phys.*, 2000, **113**, 2563-2569.

62. F. Neese, *Wiley Interdisciplinary Reviews: Computational Molecular Science*, 2012, **2**, 73.

63. F. Neese, *Wiley Interdisciplinary Reviews: Computational Molecular Science*, 2017, **8**, e1327.

64. S. Grimme, J. Antony, S. Ehrlich, H. Krieg, J. Chem. Phys. 2010, **132**, 154104.

65. M. Kohout, K. Pernal, F. R. Wagner, Yu. Grin, *Theor. Chem. Acc.*, 2004, **112**, 453-459.

66. E. R. Johnson, S. Keinan, P. Mori-Sánchez, J. Contreras-García, A. J. Cohen, W. Yang, *J. Am. Chem. Soc.*, 2010, **132**, 6498–6506.

67. M. Kohout, *DGrid, ver. 5.1*; Radebeul, 2019, http://www2.cpfs.mpg.de/~kohout/dgrid.html

68. T. Lu, F. Chen, *J. Comput. Chem*., 2012, **33**, 580-592.

69. K. Momma, F. Izumi, *J. Appl. Crystallogr*., 2011, **44**, 1272-1276.

70. W. Humphrey, A. Dalke, K. Schulten, *J. Molec. Graphics*, 1996, **14**, 33-38.